Research Article J. Electrochem. Sci. Technol., 2020, 11(4), 384-391

Preparation of Co_3O_4/NF Anode for Lithium-ion Batteries

Shiyi Tian[1], Botao Li[2], Bochao Zhang[2], Yang Wang[1], Xu Yang[2], Han Ye[2], Zhijie Xia[2] and Guoxu Zheng[2]*

[1]School of Science, Harbin University of Science and Technology, Harbin, China
[2]School of software and microelectronics, Harbin University of Science and Technology, Harbin, China

ABSTRACT

Due to its characteristics of light weight, high energy density, good safety, long service life, no memory effect, and environmental friendliness, lithium-ion batteries (LIBs) are widely used in various portable electronic products. The capacity and performance of LIBs largely depend on the performance of electrode materials. Therefore, the development of better positive and negative materials is the focus of current research. The application of metal organic framework materials (MOFs) derivatives in energy storage has attracted much attention and research. Using MOFs as precursors, porous metal oxides and porous carbon materials with controllable structure can be obtained. In this paper, rod-shaped Co-MOF-74 was grown on Ni Foam (NF) by hydrothermal method, and then Co-MOF-74/NF precursor was heat-treated to obtain rod-shaped Co_3O_4/NF. Ni Foam was skeleton structured, which effectively relieved. The change of internal stress changes and destroys the structural volume of the electrode material and reduces the capacity attenuation. Co_3O_4/NF composite material has a specific discharge capacity of up to 1858 mA h/g for the first time, and a reversible capacity of up to 902.4 mA h/g at a current density of 200 mA/g, and has excellent rate and impedance performance. The synthesis strategy reported in this article opens the way to design high-performance electrodes for energy storage and electrochemical catalysis.

Keywords : MOFs, Mixed Metal Oxide, LIBs, Electrode Materials, Co_3O_4

Received : 11 June 2020, Accepted : 6 July 2020

1. Introduction

In the past several decades, LIBs have received extensive attention due to their high energy density, its long cycle life and outstanding safety [1-2]. With the popularity of portable electronic products, the human society's demand for the popularity of portable electronic products, the human society's demand for performance LIBs is growing, and a lot of research work has been invested in exploring and developing new anode materials. Transition metal oxides have potential energy conversion and storage applications due to reversible redox reactions [3-7]. Co_3O_4 has a high theoretical capacity (890 mA h/g), good electrochemical performance and environmental friendliness, and has wide application prospects in lithium ion battery electrode materials [8-10]. When Co_3O_4 is used as a negative electrode material for lithium ion batteries, although the specific capacity for the first charge and discharge is high, its conductivity is poor, and with the progress of the charge and discharge cycle, the material itself will undergo irreversible volume expansion, resulting in poor cycle performance. The studies have found that Co_3O_4 nanomaterials with a certain morphology can increase the contact area between the material and the electrolyte, shorten the diffusion path of electrons and Li^+, and thus improve its cycle performance [11-13]. Lee Kyung Joo et al. [14] obtained plate-shaped and rod-shaped Co-MOF by controlling the reaction conditions, and further pyrolyzed Co-MOF to obtain corresponding plate-shaped and rod-shaped Co_3O_4. The rate performance is better than the plate-like Co_3O_4 material. The difference in the electrochemical performance of the two Co_3O_4 materials is mainly caused by the difference in their morphology. As a typical current collector with good electrical conductivity, Ni Foam has good electrical conductivity and

*E-mail address: tsywrqwer@163.com

DOI: https://doi.org/10.33961/jecst.2020.01095

This is an open-access article distributed under the terms of the Creative Commons Attribution Non-Commercial License (http://creativecommons.org/licenses/by-nc/4.0) which permits unrestricted non-commercial use, distribution, and reproduction in any medium, provided the original work is properly cited.

extremely high specific surface area. Its own 3D framework can support the growth of active materials and can also provide channels for ions during the electrochemical reaction process, and is a current collector material with excellent performance [15-16]. At present, the traditionally prepared Co_3O_4 electrode materials are mostly in the powder state, and it is necessary to add a polymer binder to coat the metal current collector (such as copper sheet etc.), which not only increases the process of preparing the electrode material, but also has low conductivity after the addition of the polymer binder, increases the interface resistance and internal resistance of the electrode material, resulting in a decrease in the specific capacity and cycle life of the lithium-ion battery, which significantly affect its application in the field of lithium-ion batteries [17-18]. Co_3O_4 electrode materials are grown directly on NF, which not only reduces the cost of preparation, but also does not require the introduction of high-conductivity polymers, which is conducive to the exchange of charge and the penetration of electrolyte ions, to improving the specific capacitance, rate performance and cycle stability, etc. of the material. [19-23]. In this paper, rod-shaped Co-MOF-74 was grown on NF by hydrothermal method, and then Co-MOF-74/NF precursor is calcined under certain conditions to obtain rod-shaped Co_3O_4/NF, which is characterized by a series of tests. And it was processed into the negative electrode of lithium ion battery, button battery was assembled, and its electrochemical performance was explored.

2. Experimental

2.1 Preparation of Co_3O_4/NF

A Ni Foam material with a thickness of 0.5 mm and an areal density of 280 g/m^2 was used as the substrate. All standard solutions were prepared with ultrapure water with a resistance of 18.2 MΩ at 25°C. Ni Foam was ultrasonically sonicated in HCl solution (3 M) for 30 minutes to remove the nickel oxide layer on the surface, rinsed with ultrapure water and absolute ethanol, and then dried in air. Step 1: 250 mg $Co(NO_3)_2{\cdot}6H_2O$ and 60 mg 2,5-dihydroxyterephthalic acid was dissolved in 20 mL N,N-dimethylformamide. Step 2: After 10 minutes of ultrasonic vibration, 1.2 mL of ethanol and 1.2 mL of H_2O were added to obtain a well-dispersed suspension. Step 3: the resulting solution was transferred to a 25 mL negative-pressure autoclave with polytetrafluoroethylene lining. Ni Foam was vertically immersed in the prepared solution, then the autoclave was sealed and placed in an oven at 120°C for 24 h. Finally, the autoclave was taken out and cooled naturally. The resulting product was rinsed with ethanol and dried in air to obtain Co-MOF-74/NF. The prepared Co-MOF-74/NF material was put in a muffle furnace and calcined at 400°C for 2 h to obtain Co_3O_4/NF material. The preparation flow chart is shown in Fig. 1.

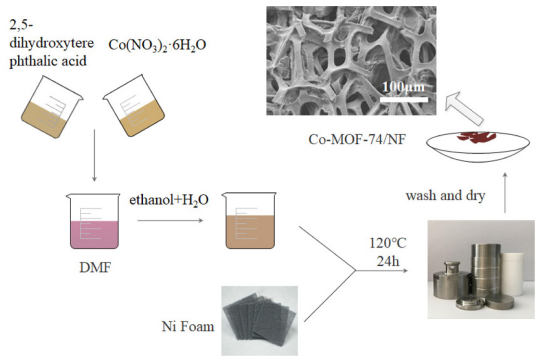

Fig. 1. Schematic diagram

2.2 Material characterization

Material characterization tests were performed by X-ray diffraction (XRD) and scanning electron microscope (SEM).

2.3 Electrochemical measurement

The electrochemical performance of Co_3O_4/NF was studied by assembling the button battery (CR2032). The process of assembling the battery was in a glove box filled with argon. The cycle performance and rate performance of the battery were tested using Wuhan Landian Battery Test System with a voltage window of 0.01-3.0 V. The cyclic voltammetry (CV) and AC impedance (EIS) of the battery were tested by the Shanghai Chenhua Electrochemical Workstation, and the reaction mechanism and impedance of the electrode materials were analyzed. CV condition: the voltage range was 0.01-3.00 V, scanning speed was 0.01 mV/s; EIS condition: the frequency range was 10 m Hz-10^6 Hz, and disturbance voltage was 5 mV.

3. Results and Discussion

X-ray analysis was applied to Co-MOF-74/NF pre-

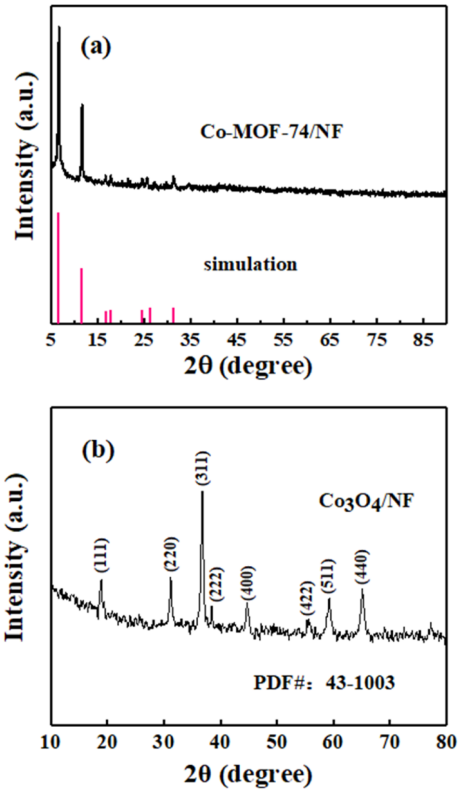

Fig. 2. XRD patterns of (a) Co-MOF-74/NF, (b) Co_3O_4/NF

cursor and Co_3O_4/NF to determine their crystal structure, as shown in Fig. 2. Fig. 2(a) is a comparison of the Co-MOF-74/NF XRD spectrum and the MOF-74 standard simulated spectrum. It can be seen from the figure that the characteristic diffraction peak of the experimentally prepared product is basically consistent with the diffraction peak of the MOF-74 single crystal simulation pattern, and the diffraction peaks were at 2θ=6.8° and 11.8°, corresponding to the (210) and (300) crystal planes of single crystal MOF-74 in the literature, respectively. There was no impurity diffraction peaks, indicating that the synthesized product is pure phase Co-MOF-74/NF, and the diffraction peaks were sharp, indicating that the prepared Co-MOF-74/NF have good crystallization performance. Fig. 2(b) is the XRD pattern of Co_3O_4/NF. It can be seen from the figure that the diffraction peaks at 2θ=44.4° correspond to the (400) crystal planes of nickel metal, which shows that the composite electrode material contains Nickel foam.

In addition, the diffraction peaks appearing at

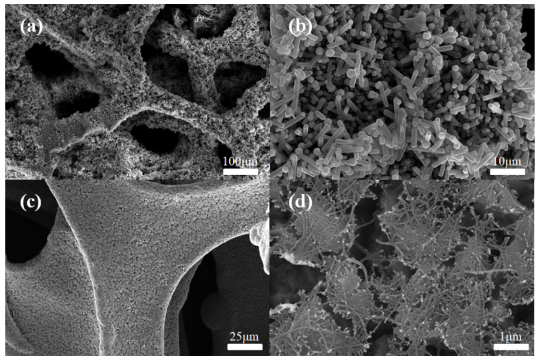

Fig. 3. SEM images of (a-b) Co-MOF-74/NF; (c-d) Co_3O_4/NF

2θ=18.9°, 31.3°, 36.7°, 38.5°, 55.8°, 59.3°, 65.2°, corresponds to the (111), (220), (311), (222), (422), (511), (440) crystal planes of the Co_3O_4 cubic crystal phase. Through the analysis of JADE software, the intensity and position of each diffraction peak are consistent with the Co_3O_4 standard card (PDF#: 43-1003). The intensity of the main diffraction peak is very high, and no other obvious impurity peaks appear, indicating the formation of Co_3O_4/NF composite electrode material.

The SEM characterization results are shown in the figure. Fig. 3(a-b) is the Co-MOF-74/NF precursor obtained after hydrothermal, and it can be seen from the figure that the Co-MOF-74/NF precursor has a rod-like structure, and the size is relatively uniform. Fig. 3(c-d) is Co_3O_4/NF obtained after heat treatment. It can be seen from the figure that the obtained metal oxide still retains the rod-like structure of its precursor, but the size is slightly reduced compared to its precursor. This is mainly due to the shrinkage of the structure caused by the decomposition of 2,5-dihydroxyterephthalic acid ligand during pyrolysis. Co_3O_4 grows on the substrate with sufficient space between it, which is conducive to the wetting of the electrolyte, and can shorten the diffusion distance of lithium ions, which is beneficial to the full use of active materials, and to some extent helps prevent Co_3O_4 from falling off the substrate during cycling.

Fig. 4 is the cyclic voltammetry curve of Co_3O_4/NF.

Its voltage sweep range is 0.01-3.0 V, and its sweep rate is 0.01 mV/s. As shown in the figure, during the first cycle of cathodic scanning, a strong reduction peak appeared at about 0.45 V, which corresponds to the reaction in which Co_3O_4 is reduced to metallic

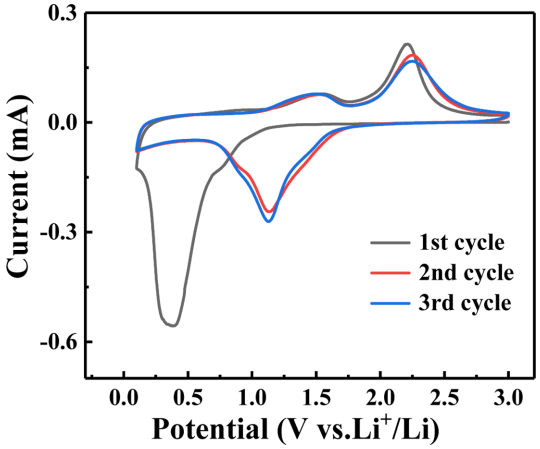

Fig. 4. Cyclic voltammetry curve of Co_3O_4/NF

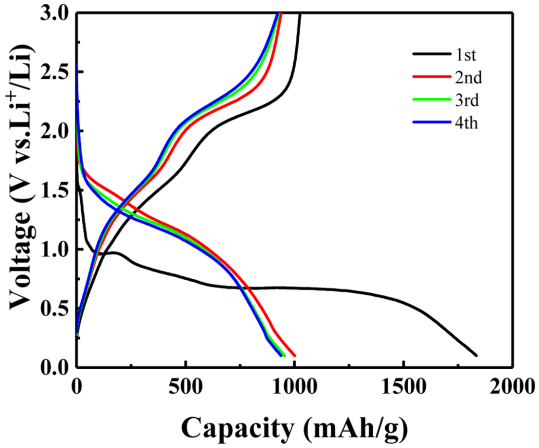

Fig. 5. Charging and discharging curves of Co_3O_4/NF

cobalt and amorphous Li_2O is formed, and to the formation procedures accompanied with electrolyte decomposition and solid electrolyte interface membrane (SEI membrane) generation [24-25]. As shown in formula (1) and (2).

$$Co_3O_4+2Li^++2e^-\rightarrow 2CoO+Li_2O \quad (1)$$

$$CoO+2Li^++2e^-\rightarrow Co+Li_2O \quad (2)$$

The main components of SEI are Li_2CoO_3, Li_2O, $ROCO_2Li$, etc. It has the characteristics of solid electrolyte, is an insulator of electrons, and an excellent conductor of Li^+. The formation of SEI film is conducive to coating the electrode, preventing short circuit, and can play a protective role on the material structure. During the first cycle of anode scanning, an obvious oxidation peak appeared at 2.2 V, corresponding to the phase transition process of the oxidation of Co to Co^{2+} and Co^{3+} [26]. As shown in formula (3) and (4).

$$Co+Li_2O\rightarrow CoO+2Li^++2e^- \quad (3)$$

$$2CoO+Li_2O\rightarrow Co_3O_4+2Li^++2e^- \quad (4)$$

In the following two cycles, the position of the reduction peak shifted, and there was a reduction peak around 1.0 V. Because the SEI film formed in the first cycle consumed a large amount of Li^+, the intensity of the reduction peak in the following two cycles was significantly weakened relative to the first cycle, the position of the oxidation peak was not changed, and the intensity was somewhat less. The redox peak of the third cycle and the redox peak of the second cycle had a good coincidence, indicating that the battery reaction entered the stable stage after the first cycle, and the SEI generated on the surface of Co_3O_4 was also stable.

Fig. 5 is the first four charge-discharge curves of Co_3O_4/NF at a current density of 200 mA/g, and the voltage range was 0.01-3.0 V. During the first discharge, there was an obvious platform at 1.0 V, corresponding to the formation reaction of Co_3O_4 reduced to metal Co and SEI, which is consistent with the results of the cyclic voltammetry curve in Fig. 4 [27]. Similarly, the first discharge appeared a platform near 2.1 V, corresponding to the oxidation peak of the cyclic voltammetry curve, which was the reaction process of the oxidation of metal Co to Co^{2+} and Co^{3+}. The first discharge and charge capacities were 1858 mA h/g and 1004 mA h/g, respectively. The irreversible capacity of the first discharge is generally considered to be related to electrolyte decomposition and SEI film formation [28]. In addition to the irreversible capacity in the first cycle, the second and third cycles maintained high capacity, 945 and 942 mA h/g, respectively, indicating that the electrochemical reaction was well reproducible, and the grass-like Co_3O_4/NF material we synthesized performed good cycle stability.

In order to study the cycling stability of the battery at a certain current density, the battery was cycled 200 times at 200 mA/g. The test results are shown in

Fig. 6. It can be clearly seen from the figure that Co_3O_4/NF had a high reversible capacity and excellent cycle performance. As shown in the figure, the initial discharge and charge specific capacities of the Co_3O_4/NF electrode reached 1858 mA h/g and 1004 mA h/g, respectively, and after 200 cycles, the discharge specific capacity could be maintained at 902.4 mA h/g. In addition, from the tenth lap, the reversible capacity of the Co_3O_4/NF electrode slowly increased, which might be caused by the following two reasons, one is the gradual decomposition of the irreversible Li_2O formed during the first charge and discharge process [29-30], the second is that during the charging and discharging process, a layer of polymer/colloid coating will be formed on the electrode surface. The formation and decomposition of these coatings lead to a slow rise in specific capacity [31-33]. During the cycle, the Coulomb efficiency was always maintained above 97%, showing excellent cycle stability. As it is known, Co_3O_4 material has a volume change during the intercalation and deintercalation of lithium, which is apt to produce powdering, which leads to the attenuation of the cycle performance. The Co_3O_4/NF synthesized in this paper has excellent cycle performance, which is closely related to stability of the structure of the electrode material. It is exactly because of the unique three-dimensional spatial structure that is beneficial to buffer the volume change of Co_3O_4 material during the cycle, it had a stable structure to ensure that enough active substances participate in the electrochemical reaction, and to maintain a high specific capacity, thereby, showed excellent cycle performance.

The battery was each placed under different current densities for 10 cycles to test the rate performance of the battery, as shown in Fig. 7. At 200 mA/g, the Co_3O_4/NF electrode exhibited a capacity of 889 mA h/g. As the current density increased, the capacity gradually decreased. At a current density of 400 mA/g, 600 mA/g, 800 mA/g, the capacities at 1000 mA/g were 760 mA h/g, 643 mA h/g, 568 mA h/g, and 503 mA h/g. Even at a current density of 1000 mA/g, the Co_3O_4/NF electrode could still maintain a high capacity (503 mA h/g). This excellent rate performance is much better than similar Co_3O_4 materials

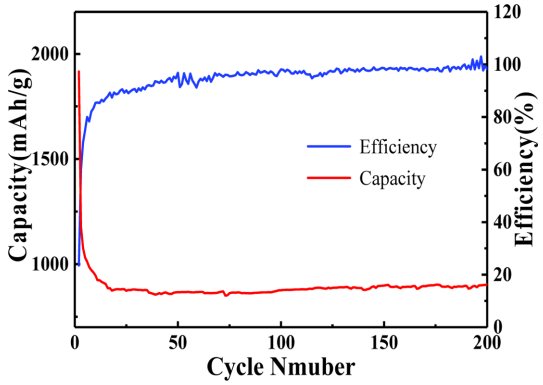

Fig. 6. Cyclic performance curves of Co_3O_4/NF

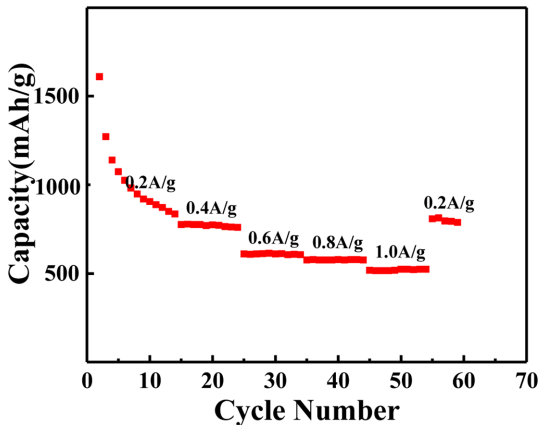

Fig. 7. Cyclic performance curves of Co_3O_4/NF

Table 1. Comparison of performance

Typical examples	Current density	Capacity	Ref.
Co_3O_4/NF	200 mA/g	902.4 mA h/g after 200 cycles	This work
Co_3O_4/NF	1000 mA/g	503 mA h/g after 50 cycles	This work
Co_3O_4-C	200 mA/g	712 mA h/g after 30 cycles	[34]
Co_3O_4	100 mA/g	743 mA h/g after 50 cycles	[35]
Co_3O_4 @MnO_2	1000 mA/g	387mA h/g after 45 cycles	[36]

reported in many literatures [34-36]. As shown in Table 1. More importantly, after the rate performance test was completed, the battery discharge capacity could be fully recovered and slightly improved (902 mA h/g) when the current density became 200 m A/g. The above further illustrates that the excellent rate performance and reversible performance of Co_3O_4/NF. The excellent rate performance shall be attributed to that the Co_3O_4/NF electrode material provides a large specific surface area, more electrochemically active sites, three-dimensional space spatial structure interpenetrating each other to form intersecting pores, speeding up the transfer rate of ions and charges.

As shown in Fig. 8, the impedance spectrum includes two components, a semi-circular area in the high frequency area and a straight line in the low frequency area. For the transition metal oxide anode material, the semi-circular area represents the resistance of SEI film and charge transfer resistance [37]. In the low frequency area, there is a slanted straight line, which represents the Warburg impedance caused by the material transfer, which is related to the diffusion resistance of Li^+ in the electrode material [38]. The figure shows the diameter of the semicircle in the high-frequency region of Co_3O_4/NF is smaller than the curve radius of Co_3O_4, revealing its lower impedance value and higher charge transfer efficiency. This is mainly because the three-dimensional spatial structure can effectively shorten the diffusion path of lithium ions and reduce the diffusion resistance of lithium ions.

The model of lithium insertion mechanism in Co_3O_4/NF array material is shown in Fig. 9. The lithium storage mechanism of Co_3O_4 material is the conversion mechanism, and the reaction equation (5) is as follows:

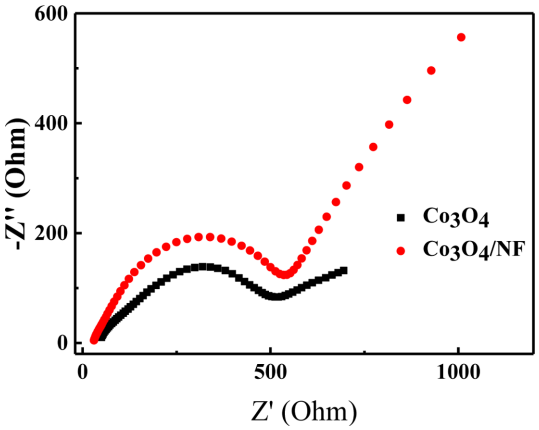

Fig. 8. AC impedance sectroscopy of Co_3O_4 and Co_3O_4/NF

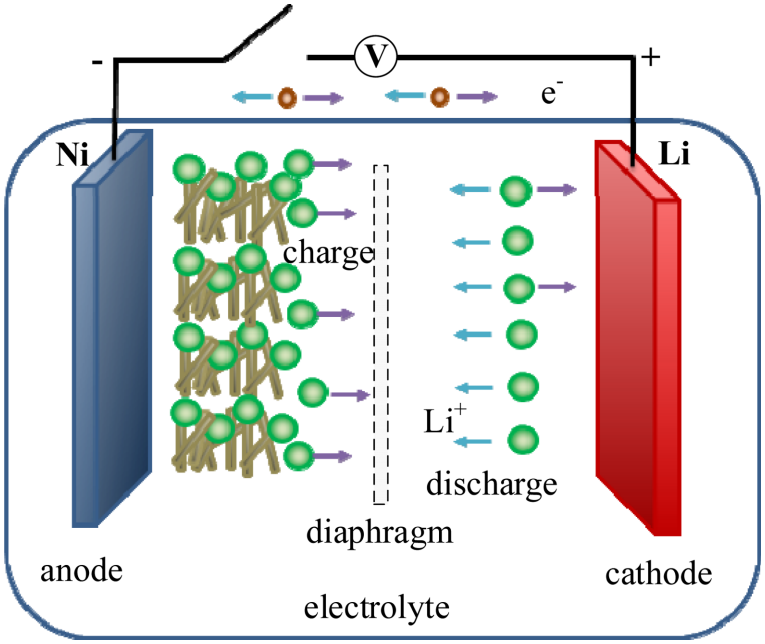

Fig. 9. Lithium inserting mechanism

$$Co_3O_4+8Li^++8e^- \leftrightarrow 4Li_2O+3Co \quad (5)$$

during the discharge process, Co_3O_4 reacts with lithium ions, being reduced to metallic Co, and amorphous lithium oxide (Li_2O) is produced; during charging, metallic Co reacts with lithium oxide (Li_2O) to produce Co_3O_4 and lithium ions. In the entire procedure of the reaction, there are reversible redox of Co_3O_4, and the formation and decomposition of Li_2O. Ni Foam base material can provide strong support, ensure the stability of the electrode in the charge and discharge cycle, reduce the charge transfer resistance, and improve the electron and ion transport efficiency. The arrays are staggered to form a three-dimensional channel, which improves the speed of lithium ion insertion and extraction. For the Co_3O_4/NF composite electrode material, the array structure appears during the cycle, which improves the contact probability of the rod-shaped Co_3O_4, which is more conducive to improving the electron transmission capacity and forming a more stable structure. The three-dimensional space structure can increase the insertion/extraction speed of lithium ions, increase the lithium storage capacity per unit volume of composite materials, and improve the transfer efficiency of charges in electrochemical reactions.

4. Conclusions

Co_3O_4/NF composite material was successfully prepared by hydrothermal method. The microscopic morphology and crystal structure of the material were tested by XRD and SEM. The prepared Co_3O_4/NF composite material showed a rod-like structure and the size was relatively uniform. The needle-shaped Co_3O_4 electrode material was electrochemically tested. The first discharge specific capacity of Co_3O_4/NF composite material was up to 1858 mA h/g, and the reversible capacity was up to 902.4 mA h/g at a current density of 200 mA/g, and it had excellent rate and impedance performance. Co_3O_4/NF composite material, as the battery anode material, showed excellent performance, which is mainly due to the three-dimensional spatial structure, resulting in many pores in the electrode material. These pores can serve as a volume expansion buffer space for the electrode material during lithium ion insertion/extraction process, alleviating the internal stress of the electrode material. The presence of pores also increased the electrode/electrolyte contact area, resulting in that the electrochemical reaction could fully proceed in an easier manner. The strong Foam Ni skeleton structure not only guaranteed higher charge transfer efficiency in the electrochemical process, but also served as a strong support matrix for Co_3O_4 material, preventing the occurrence of agglomeration.

Acknowledgment

The authors acknowledge financial support from Natural Science Foundation of China (51502063), China Postdoctoral Science Foundation (2016T90306 and 2015M570301), Natural Science Foundation (E2015064) and Postdoctoral Science Foundation (LBH-TZ0615) of Heilongjiang Province of China, Natural Science Foundation of Heilongjiang Province of China (Geant No.F2017017),and Science Funds for Young Innovative Talents of HUST (201505). National undergraduate innovation and entrepreneurship training program (project No.201910214016 and No.201910214005).

References

[1] K. Kang, Y.S. Meng, J. Breger, *Science*, **2006**, *311(5763)*, 977-980.
[2] J.Y. Luo, H.M. Xiong, Y.Y. Xia, *J. Phys. Chem. C*, **2008**, *112(31)*, 12051-12057.
[3] T. Brezesinski, J. Wang, S.H. Tolbert, B. Dunn, *Nat. Mater.*, **2010**, *9(2)*, 146-151.
[4] X. Deng, H. Tueysuez, *ACS Catal.*, **2014**, *4*, 3701-3714.
[5] X. Zhu, C. Tang, H.F. Wang, Q. Zhang, C. Yang, F. Wei, *J. Mater. Chem. A*, **2015**, *3(48)*, 24540-24546.
[6] S. Tian, G. Zheng, Q. Liu, M. Ren, J. Yin, *Int. J. Electrochem. Sci.*, **2019**, *14*, 9459-9467.
[7] X.H. Xia, J.P. Tu, Y.Q. Zhang, X.L. Wang, C.D. Gu, X.B. Zhao, H.J. Fan, *ACS Nano*, **2012**, *6(6)*, 5531-5538.
[8] X. Xiao, X. Liu, H. Zhao, *Adv. Mater.*, **2012**, *24(42)*, 5762-5766.
[9] J.R. Miller, P. Simon, *Science*, **2008**, *321(5889)*, 651-652.
[10] G. Wang, L. Zhang, J. Zhang, *Chem. Soc. Rev.*, **2012**, *41(2)*, 797-828.
[11] L. Peng, Y. Ouyang, W. Li, *Electrochim. Acta*, **2016**, *190*, 126-133.
[12] N. Yan, L. Hu, Y. Li, *J. Phys. Chem. C*, **2012**, *116(12)*, 7227-7235.
[13] K. Feng, H.W. Park, X. Wang, *Electrochim. Acta*, **2014**, *139*, 145-151.
[14] K.J. Lee, T.H. Kim, T.K. Kim, *J. Mater. Chem. A*, **2014**, *2(35)*, 14393-14400.

[15] F. Du, D. Yu, L. Dai, *Chem. Mater.*, **2011**, *23(21)*, 4810-4816.
[16] J. Xu, Q. Wang, X. Wang, *ACS Nano*, **2013**, *7(6)*, 5453-5462.
[17] L.L. Zhang, X.S. Zhao, *Chem. Soc. Rev.*, **2009**, *38(9)*, 2520-2531.
[18] K. Cheng, F. Yang, G. Wang, *J. Mater. Chem. A*, **2013**, *1(5)*, 1669-1676.
[19] H. Zhang, Y. Chen, W. Wang, *J. Mater. Chem. A*, **2013**, *1(30)*, 8593-8600.
[20] H. Lee, Y.J. Dong, J.L. Dong, *J. Mater. Chem. A*, **2014**, *2(30)*, 11891-11898.
[21] K. Qiu, H. Yan, D. Zhang, *Electrochim. Acta*, **2014**, *141*, 248-254.
[22] K. Qiu, Y. Lu, J. Cheng, *Electrochim. Acta*, **2015**, *157*, 62-68.
[23] J. Zheng, B. Zhang, *Ceram. Int.*, **2014**, *40(7)*, 11377-11380.
[24] G. Zhou, L. Li, Q. Zhang, *Phys. Chem. Chem. Phys.*, **2013**, *15(15)*, 5582-5587.
[25] P. Zhang, Z.P. Guo, Y. Huang, *J. Power Sources*, **2011**, *196(16)*, 6987-6991.
[26] W. Mei, J. Huang, L. Zhu, *J. Mater. Chem.*, **2012**, *22(18)*, 9315-9321.
[27] X. Wang, L. Yu, X.L. Wu, *J. Phys. Chem. C*, **2009**, *113(35)*, 15553-15558.
[28] Y. Fan, H. Shao, J. Wang, *Chem. Commun.*, **2011**, *47(12)*, 3469-3471.
[29] Y. Lou, J. Liang, Y. Peng, *Phys. Chem. Chem. Phys.*, **2015**, *17(14)*, 8885-8893.
[30] J. Zhu, L. Bai, Y. Sun, *Nanoscale*, **2013**, *5(12)*, 5241-5246.
[31] N. Yan, L. Hu, Y. Li, *J. Phys. Chem. C*, **2012**, *116(12)*, 7227-7235.
[32] G. Zhou, D.W. Wang, F. Li, *Chem. Mater.*, **2010**, *22(18)*, 5306-5313.
[33] J.S. Do, C.H. Weng, *J. Power Sources*, **2005**, *146(1-2)*, 482-486.
[34] J. Chen, X.H. Xia, J.P. Tu, *J. Mater. Chem.*, **2012**, *22(30)*, 15056-15061.
[35] C.C. Li, Q.H. Li, L.B. Chen, *J. Mater. Chem.*, **2011**, *21(32)*, 11867-11872.
[36] D. Kong, J. Luo, Y. Wang, *Adv. Funct. Mater.*, **2014**, *24(24)*, 3815-3826.
[37] X. Huang, X. Li, H. Wang, *Electrochim. Acta*, **2010**, *55(24)*, 7362-7366.
[38] F. Zheng, D. Zhu, Q. Chen, *ACS Appl. Mater. Inter.*, **2014**, *6(12)*, 9256-9264.